Journal of Sound and Vibration (2002) **253**(2), 447–469
doi:10.1006/jsvi.2001.4064, available online at http://www.idealibrary.com on IDEAL®

NON-LINEAR AEROELASTIC ANALYSIS USING THE POINT TRANSFORMATION METHOD, PART 1: FREEPLAY MODEL

L. Liu† and Y. S. Wong

Department of Mathematical Sciences, University of Alberta, Edmonton, Alta. Canada T6G 2G1.
E-mail: lliu@math.ualberta.ca

AND

B. H. K. Lee

Institute for Aerospace Research, National Research Council, Ottawa, Ont., Canada K1A 0R6

(*Received* 6 *March* 2001, *and in final form* 20 *September* 2001)

A point transformation technique is developed to investigate the non-linear behavior of a two-dimensional aeroelastic system with freeplay models. Two formulations of the point transformation method are presented, which can be applied to accurately predict the frequency and amplitude of limit cycle oscillations. Moreover, it is demonstrated that the developed formulations are capable of detecting complex aeroelastic responses such as periodic motions with harmonics, period doubling, chaotic motions and the coexistence of stable limit cycles. Applications of the point transformation method to several test examples are presented. It is concluded that the formulations developed in this paper are efficient and effective.

1. INTRODUCTION

The study of the dynamic behavior of aircraft structures is a crucial step in flutter analysis, since such research provides important information related to the efficient and safe design of aircraft wings and control surfaces. To investigate the dynamic response of aircraft structures, non-linear analysis is needed to take into account the effects due to structural non-linearities that occur in the restoring forces [1–5]. A detailed study on the non-linear aeroelastic behavior of airfoils was presented in a recent review paper by Lee *et al.* [6]. There are three fundamental types of concentrated structural non-linearities: cubic, freeplay and hysteresis stiffnesses. In our previous work [7], we studied a self-excited two-degree-of-freedom (d.o.f.) aeroelastic system with a cubic restoring force. Through the application of the center manifold theory and the principle of normal form, analytical formulas are derived which are capable of accurately predicting the frequencies and amplitudes of limit cycle oscillations. The goal of this paper is to continue our earlier study to develop a mathematical technique for freeplay models. The investigation for hysteresis models will be presented in Part 2 [8].

An aeroelastic model with freeplay has been investigated using analytical methods based on describing function and harmonic balance methods, and numerical techniques using

†Present address: Institute for Aerospace Research, Uplands U-66, National Research Council, Ottawa, ON, Canada K1A 0R6. E-mail: liping.liu@nrc.ca.

0022-460X/02/$35.00

time-integration schemes [1, 4, 9]. The non-linear behavior of such systems has also been studied numerically and experimentally by Conner *et al.* [10] and Tang and Dowell [11]. Although it seems that our earlier technique based on the center manifold theory can still be applied if we replace the freeplay models by polynomial or rational polynomial approximations, a detailed investigation carried out by Liu [12] has led to the conclusion that such an approach should not be used for two reasons. First, it is important to note that one feature of the freeplay is the existence of switching points in which changes in linear subdomains occur. Since a slight change in the system parameters could affect the non-linear aeroelastic behavior considerably, replacing a freeplay by a numerical approximation, which eliminates the switching points, would cause the location of the bifurcation point to be no longer exact. Second, since initial conditions play an important role in the dynamic response of aeroelastic systems with freeplay non-linearity for some range of airfoil parameters, the center manifold method, which does not take into account any information due to initial conditions, would not be expected to provide a good prediction for a freeplay or a hysteresis model.

Time-integration methods have often been used to study the response of an aeroelastic system with freeplay restoring forces. It should be noted that, for a piecewice linear system such as a freeplay model, it is not straightforward to analyze the stability of the numerical schemes, because some of the eigenvalues corresponding to one of the linear subsystems may have positive real parts. Furthermore, the standard time-integration scheme with uniform time step cannot precisely locate the switching point where the change in linear regions occurs. The importance of capturing switching points was noted by Lin and Cheng [13] and Conner *et al.* [10]. Lin and Cheng [13] reported an example showing that an entirely incorrect asymptotic behavior for a non-linear flutter can occur due to the error in capturing the switching point in the Runge–Kutta numerical scheme. A detailed study of the error analysis of the Runge–Kutta scheme for the aeroelastic system with non-linear structures has been carried out by Liu *et al.* [14], which shows that the significant differences between the exact motion and the numerical solution may be observed for some cases. However, for the cases discussed in this paper, the error caused by the inexact location of the switching points are very small by keeping the time step small.

In this paper, we introduce a mathematical technique based on the point transformation method [15]. Two formulations are developed to investigate the non-linear aeroelastic model with a freeplay non-linearity. One attractive feature of the present approach compared with a numerical time-integration scheme is that the formulations track the system behavior to the exact point where the change in linear subdomains occurs. Moreover, the solution corresponding to each linear region is determined analytically. It will be demonstrated that the formulations developed are efficient and effective. Not only can they accurately predict the amplitude and frequency of the limit cycle oscillations, but also they are capable of detecting complex non-linear aeroelastic behavior such as periodic motion with harmonics, periodic doubling, chaotic motion and the coexistence of stable limit cycles.

2. THE MATHEMATICAL MODEL

Figure 1 shows a sketch of an airfoil oscillating in plunge and pitch. The mathematical formulation for the self-excited two d.o.f. motion can be expressed as

$$\xi'' + x_\alpha \alpha'' + 2\zeta_\xi \frac{\bar{\omega}}{U^*} \xi' + \left(\frac{\bar{\omega}}{U^*}\right)^2 G(\xi) = -\frac{1}{\pi\mu} C_L(\tau),$$

$$\frac{x_\alpha}{r_\alpha^2} \xi'' + \alpha'' + 2\zeta_\alpha \frac{1}{U^*} \alpha' + \left(\frac{1}{U^*}\right)^2 M(\alpha) = \frac{2}{\pi\mu r_\alpha^2} C_M(\tau), \tag{1}$$

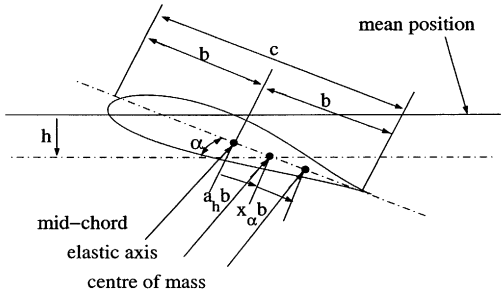

Figure 1. The sketch of an airfoil motion with two d.o.f.

where the plunge deflection is denoted by h, positive in the downward direction, and the pitch angle about the elastic axis is denoted by α, positive with nose up. The elastic axis is located at a distance $a_h b$ from the mid-chord where b is the half-chord, while the mass center is located at a distance $x_\alpha b$ from the elastic axis. $\xi = h/b$ is the non-dimensional displacement of the elastic axis, and the $'$ denotes differentiation with respect to the non-dimensional time which is defined as $\tau = Ut/b$. U^* is a non-dimensional velocity defined as $U^* = U/(b\omega_\alpha)$, where U is the velocity, and $\bar{\omega}$ is given by $\bar{\omega} = \omega_\xi/\omega_\alpha$, where ω_ξ and ω_α are the natural frequencies of the uncoupled plunging and pitching modes respectively. ζ_ξ and ζ_α are the damping ratios, and r_α is the radius of gyration about the elastic axis. μ is the airfoil/air mass ratio defined as $m/(\pi\rho b)$. $G(\xi)$ and $M(\alpha)$ represent the non-linear plunge and pitch stiffness terms respectively. For an incompressible flow, the lift and pitching moment coefficients $C_L(\tau)$ and $C_M(\tau)$ are given by [16]

$$C_L(\tau) = \pi(\xi'' - a_h\alpha'' + \alpha') + 2\pi\left\{\alpha(0) + \xi'(0) + \left(\frac{1}{2} - a_h\right)\alpha'(0)\right\}\phi(\tau)$$

$$+ 2\pi\int_0^\tau \phi(\tau - \sigma)\left(\alpha'(\sigma) + \xi''(\sigma) + \left(\frac{1}{2} - a_h\right)\alpha''(\sigma)\right)\mathrm{d}\sigma,$$

$$C_M(\tau) = \pi\left(\frac{1}{2} + a_h\right)\left\{\alpha(0) + \xi'(0) + \left(\frac{1}{2} - a_h\right)\alpha'(0)\right\}\phi(\tau)$$

$$+ \pi\left(\frac{1}{2} + a_h\right)\int_0^\tau \phi(\tau - \sigma)\left\{\alpha'(\sigma) + \xi''(\sigma) + \left(\frac{1}{2} - a_h\right)\alpha''(\sigma)\right\}\mathrm{d}\sigma$$

$$+ \frac{\pi}{2}a_h(\xi'' - a_h\alpha'') - \left(\frac{1}{2} - a_h\right)\frac{\pi}{2}\alpha' - \frac{\pi}{16}\alpha'',$$

where the Wagner function $\phi(\tau)$ is given by $\phi(\tau) = 1 - \psi_1 e^{-\varepsilon_1\tau} - \psi_2 e^{-\varepsilon_2\tau}$ with $\psi_1 = 0{\cdot}165$, $\psi_2 = 0{\cdot}335$, $\varepsilon_1 = 0{\cdot}0455$ and $\varepsilon_2 = 0{\cdot}3$.

Through the introduction of four new variables $w_1 = \int_0^\tau e^{-\varepsilon_1(\tau-\sigma)}\alpha(\sigma)\,\mathrm{d}\sigma$, $w_2 = \int_0^\tau e^{-\varepsilon_2(\tau-\sigma)}\alpha(\sigma)\,\mathrm{d}\sigma$, $w_3 = \int_0^\tau e^{-\varepsilon_1(\tau-\sigma)}\xi(\sigma)\,\mathrm{d}\sigma$, and $w_4 = \int_0^\tau e^{-\varepsilon_2(\tau-\sigma)}\xi(\sigma)\,\mathrm{d}\sigma$, the original integro-differential equations for the self-excited aeroelastic system (1) can be reformulated into a set

of autonomous differential equations as $X' = f(X)$, where $X = \{x_1, x_2, x_3, x_4, x_5, x_6, x_7, x_8\} = \{\alpha, \alpha', \xi, \xi', w_1, w_2, w_3, w_4\} \in R^8$. Explicitly, the system can be written as

$$
\begin{aligned}
x_1' &= x_2,\\
x_2' &= a_{21}x_1 + a_{22}x_2 + a_{23}x_3 + a_{24}x_4 + a_{25}x_5 + a_{26}x_6 + a_{27}x_7\\
&\quad + a_{28}x_8 + j\left(d_0\left(\frac{\bar{\omega}}{U^*}\right)^2 G(x_3) - c_0\left(\frac{1}{U^*}\right)^2 M(x_1)\right),\\
x_3' &= x_4,\\
x_4' &= a_{41}x_1 + a_{42}x_2 + a_{43}x_3 + a_{44}x_4 + a_{45}x_5 + a_{46}x_6 + a_{47}x_7\\
&\quad + a_{48}x_8 + j\left(c_1\left(\frac{1}{U^*}\right)^2 M(x_1) - d_1\left(\frac{\bar{\omega}}{U^*}\right)^2 G(x_3)\right),\\
x_5' &= x_1 - \varepsilon_1 x_5, \quad x_6' = x_1 - \varepsilon_2 x_6, \quad x_7' = x_3 - \varepsilon_1 x_7, \quad x_8' = x_3 - \varepsilon_2 x_8,
\end{aligned}
\tag{2}
$$

where the coefficients j, $a_{21}, \ldots, a_{28}$, $a_{41}, \ldots, a_{48}$, c_0, d_0, c_1 and d_1 are related to the system parameters and their expressions are given in Appendix A.

The structural non-linearities are represented by the non-linear functions $G(x_3)$ and $M(x_1)$ in system (2). Generally speaking, for a freeplay model, $M(x_1)$ is given by

$$
M(x_1) = \begin{cases} M_0 + x_1 - \alpha_f, & x_1 < \alpha_f,\\ M_0 + M_f(x_1 - \alpha_f), & \alpha_f \leqslant x_1 \leqslant \alpha_f + \delta,\\ M_0 + x_1 - \alpha_f + \delta(M_f - 1), & x_1 > \alpha_f + \delta, \end{cases}
\tag{3}
$$

where M_0, M_f, α_f and δ are constants. Here, we give the expressions for $M(x_1)$ in the pitch d.o.f. Similar expressions for $G(x_3)$ in the plunge motion can be written by replacing x_1 with x_3. The sketch of the freeplay model is given in Figure 2.

Consider the eight-dimensional system given in equation (2) for a freeplay spring in pitch and a linear spring in plunge, where $M(x_1)$ is given by equations (3) and $G(x_3) = \beta x_3$. According to the three linear branches of the bilinear function for a freeplay model, the

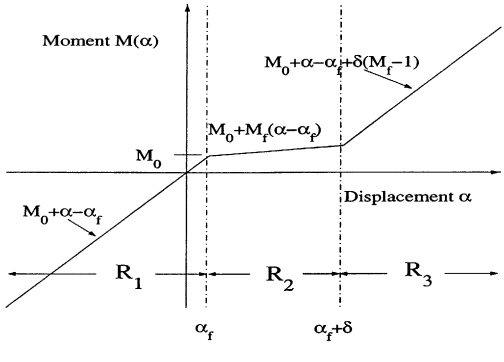

Figure 2. General sketch of a freeplay stiffness.

phase space $X \in R^8$ can be divided into three regions, R_i $(i = 1, 2, 3)$, where each corresponds to a linear system:

$$X' = AX + F_1 \quad \text{in } R_1 = \{X \in R^8 | x_1 < \alpha_f\},$$

$$X' = BX + F_2 \quad \text{in } R_2 = \{X \in R^8 | \alpha_f < x_1 < \alpha_f + \delta\},$$

$$X' = AX + F_3 \quad \text{in } R_3 = \{X \in R^8 | x_1 > \alpha_f + \delta\}.$$

Here A and B are 8×8 constant matrices, and F_1, F_2 and F_3 are 8×1 constant vectors. The elements of A, B and F_i $(i = 1, 2, 3)$ are determined by the system parameters of the coupled aeroelastic equations, and they are given by

$$A = \begin{pmatrix} A_1 & A_2 \\ A_3 & A_4 \end{pmatrix}, \qquad B = \begin{pmatrix} B_1 & A_2 \\ A_3 & A_4 \end{pmatrix}$$

and $F_1 = (M_0 - \alpha_f)F$, $F_2 = (M_0 - M_f\alpha_f)F$, $F_3 = (M_0 - \alpha_f + \delta_0(M_f - 1))F$. The elements of the 4×4 block matrices, A_i $(i = 1, 2, 3, 4)$, B_1, and the vector F are defined in Appendix B.

3. POINT TRANSFORMATION METHOD

Consider the freeplay model shown in Figure 2. Let the Z–Y plane represent the eight-dimensional phase space, where $Z = \{x_1\}$ and $Y = \{x_2, x_3, x_4, x_5, x_6, x_7, x_8\}$. The Z–Y phase space is now divided into three regions R_1, R_2 and R_3 according to the subspaces $Z = \alpha_f$ and $Z = \alpha_f + \delta$ as shown in Figure 3(a). The system response can then be predicted by following a general phase path. Assuming that a motion initially starts at a point X_0 as shown in Figure 3(a), the trajectory begins in R_1 and passes through R_2 into R_3. Then it returns through R_2 back into R_1. Let X_1 and X_2 be the points through which the trajectory enters R_2 and R_3 respectively. Let X_3 and X_4 be the points through which the trajectory leaves R_3 and R_2 respectively. These points (X_1, X_2, X_3 and X_4) are called switching points, since they locate the places where the linear systems change. Let t_1 be the travelling time of the trajectory (from X_1 to X_2) in region R_2. Similarly, let t_2, t_3 and t_4 be the

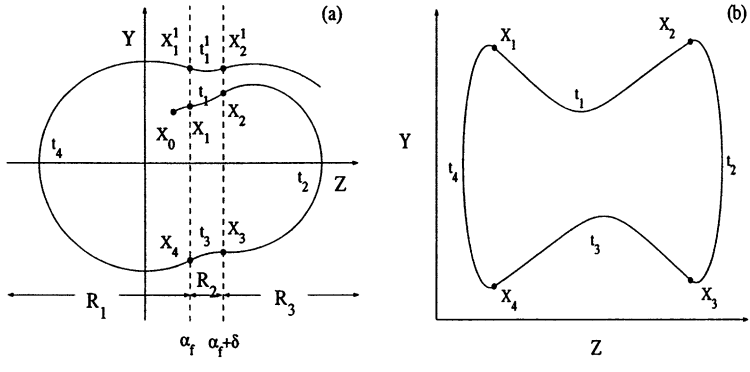

Figure 3. General trajectory (a) and a period-one trajectory (b) of system (2) with a freeplay stiffness in pitch.

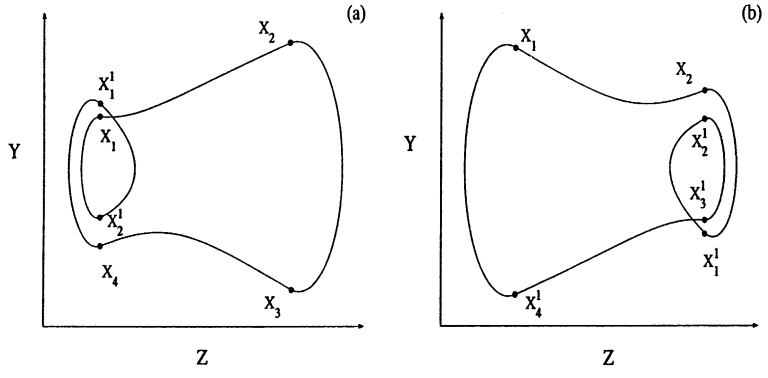

Figure 4. Trajectories for system (2) with a freeplay stiffness in pitch: period-one with harmonics where (a) the smaller loop covers R_1 and R_2; (b) the smaller loop covers R_2 and R_3.

travelling times of the trajectory in regions R_3, R_2 and R_1 respectively. The above process of the point transformation is then repeated. When a steady state is reached, the trajectory may consist of only four switching points X_1, X_2, X_3, X_4 and four travelling times t_1, t_2, t_3 and t_4 as illustrated in Figure 3(b).

It should be noted that the system of equations in each region is strictly linear. Hence, the exact solutions in R_1, R_2 and R_3 can be expressed analytically. Using the analytical solutions in different regions, we can determine the maximum and minimum values of α corresponding to $\alpha' = 0$. Moreover, based on the information provided by the switching points, travelling times and the maximum and minimum amplitudes for α, we can predict the type of steady state motion for the aeroelastic system. For instance, when the transients have diminished, we may observe a repetition of the switching points X_1, X_2, X_3, X_4 and the corresponding travelling times t_1, t_2, t_3, t_4 covering the entire region as shown in Figure 3(b). Then, the steady state motion is classified as a limit cycle oscillation (LCO) with one frequency. The existence of one frequency component is further confirmed by only one maximum and one minimum value for α. The frequency can be determined by $f = 1/T$, where T denotes the period which is the sum of the travelling times (i.e., $T = \sum_{i=1}^{4} t_i$). The resulting LCO is of period-one, and the trajectory illustrated in Figure 3(b) has one complete loop covering the three regions R_1, R_2 and R_3.

The point transformation method is capable of predicting more general periodic motions. Note that it is not necessary that the switching points appear in the sequence as shown in Figure 3(b). For example, the steady state trajectory displayed in Figure 4(a) which contains six switching points. The additional two points X_1^1 and X_2^1 are introduced after completing the sequence discussed previously. In this case, a complete loop consists of six points, X_1, X_2, X_3, X_4, X_1^1, X_2^1, and six corresponding travelling times, t_1, t_2, t_3, t_4, t_1^1, t_2^1. Unlike the trajectory shown in Figure 3(b), the complete loop covering the entire region also contains a smaller loop covering two regions R_1 and R_2. The smaller loop is defined as the one covering only one or two regions. The resulting LCO is of period-one, since we observe only one complete loop covering the entire region. However, the presence of a smaller loop indicates that the LCO has a harmonic component. Since the LCO is of period-one, the frequency is estimated by $f = 1/T$ where $T = \sum_{i=1}^{4} t_i + \sum_{i=1}^{2} t_i^1$. The typical feature of an LCO with harmonics can be verified by four values for α when $\alpha' = 0$. Recall that for a period-one LCO with one frequency, only two values of α corresponding to $\alpha' = 0$ exist. Figure 4(b) illustrates a similar situation, but with the two extra switching points X_2^1 and X_3^1 due to the presence of a smaller loop covering regions R_2 and R_3.

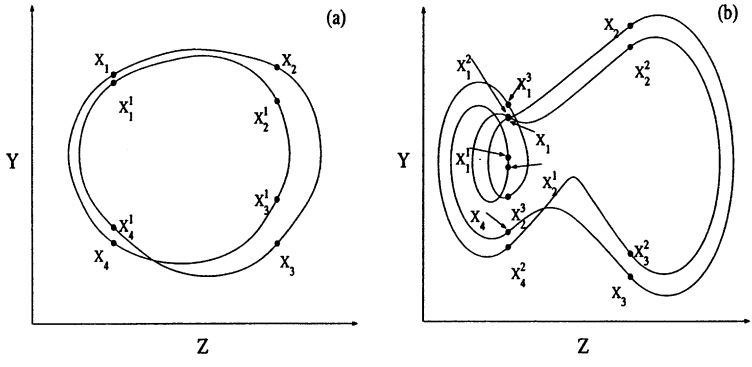

Figure 5. Trajectories for system (2) with a freeplay stiffness in pitch: period-two LCO (a) without harmonics and (b) with harmonics where two smaller loops cover R_1 and R_2.

The predicted LCOs discussed in Figures 3 and 4 are of period-one, since the point transformation confirms the presence of only one complete loop covering the entire region. If, however, a complete loop covers the entire region n times, the LCO is classified as a period-n LCO and the frequency is given by $f = 1/T$, where the period T is the sum of the travelling times. For example, Figures 5(a) and 5(b) display period-two LCOs. Figure 5(a) corresponds to a simple period-two LCO, and the trajectory contains eight switching points and eight travelling times in a complete loop. In Figure 5(b), a complete loop contains two smaller loops, indicating that the period-two LCO has harmonic components. If the sequence of switching points does not repeat after a sufficiently long time, the motion may be classified as chaos.

In summary, the point transformation method can be used to detect a general period-n LCO for an aeroelastic system with freeplay. Moreover, it can predict the presence of harmonic components and is also capable of determining the frequency and the maximum and minimum amplitudes of an LCO.

In the following sections, we present two formulations based on the above discussion. Then the formulations developed will be applied to predict the non-linear aeroelastic behavior for a freeplay model.

3.1. FORMULATION 1

This formulation begins with a given set of initial conditions X_0. First, the travelling times are determined by solving a non-linear equation. Then, the switching points are calculated by the multiplication of a known matrix by a known vector, which will be further explained after the formulation is presented. If the round-off error can be neglected, the formulation will produce the exact solution for the aeroelastic system. The detailed procedure is given as follows.

Step 0: Set the initial vector $X_0 = (x_{01}, x_{02}, x_{03}, \ldots, x_{08})^{\mathrm{T}}$. Let $i = 1$ for $\alpha_f < x_{01} < \alpha_f + \delta$ and $x_{02} > 0$, $i = 2$ for $x_{01} > \alpha_f + \delta$, $i = 3$ for $\alpha_f < x_{01} < \alpha_f + \delta$ and $x_{02} < 0$, and $i = 4$ for $x_{01} < \alpha_f$. Set $X_i = X_0$, and go to step i.

Step 1: Solve the non-linear equations $\alpha_f + \delta = \{e^{Bt}X_1 + \mathscr{B}(t)F_2\}|_{(1)}$ and $\alpha_f = \{e^{Bt}X_1 + \mathscr{B}(t)F_2\}|_{(1)}$ separately for t. Here, $\{V\}|_{(n)}$ denotes the nth element of the vector V. Let the smallest positive solutions corresponding to the first and second equations be t^* and t^{**} respectively. If $t^* < t^{**}$, let $t_1 = t^*$, compute X_2 using $X_2 = e^{Bt_1}X_1 + \mathscr{B}(t_1)F_2$, and go to step 2. If $t^{**} < t^*$, let $t_3 = t^{**}$, compute X_4 using $X_4 = e^{Bt_3}X_1 + \mathscr{B}(t_3)F_2$, and go to step 4.

Step 2: First, solve $\{e^{At}X_2 + \mathscr{A}(t)F_3\}|_{(2)} = 0$ for t, assign the smallest positive value to t_u, and compute the maximum amplitude by $\alpha_{max} = \{e^{At_u}X_2 + \mathscr{A}(t_u)F_3\}|_{(1)}$. Then, solve $\alpha_f + \delta = \{e^{At}X_2 + \mathscr{A}(t)F_3\}|_{(1)}$ for t, assign the smallest positive value to t_2, and compute X_3 using $X_3 = e^{At_2}X_2 + \mathscr{A}(t_2)F_3$. Go to step 3.

Step 3: Similar to step 1, solve the non-linear equations $\alpha_f = \{e^{Bt}X_3 + \mathscr{B}(t)F_2\}|_{(1)}$ and $\alpha_f + \delta = \{e^{Bt}X_3 + \mathscr{B}(t)F_2\}|_{(1)}$ separately for t. Let the smallest positive solutions corresponding to the first and second non-linear equations be t^* and t^{**} respectively. If $t^* < t^{**}$, let $t_3 = t^*$, compute X_4 using $X_4 = e^{Bt_3}X_3 + \mathscr{B}(t_3)F_2$, and go to step 4. If $t^{**} < t^*$, let $t_1 = t^{**}$, compute X_2 using $X_2 = e^{Bt_1}X_3 + \mathscr{B}(t_1)F_2$, and go to step 2.

Step 4: Similar to step 2, first solve $\{e^{At}X_4 + \mathscr{A}(t)F_1\}|_{(2)} = 0$ for t, assign the smallest positive value to t_l, and compute the minimum amplitude by $\alpha_{min} = \{e^{At_l}X_4 + \mathscr{A}(t_l)F_1\}|_{(1)}$. Then, solve $\alpha_f = \{e^{At}X_4 + \mathscr{A}(t)F_1\}|_{(1)}$ for t, assign the smallest positive value to t_4, and compute X_1 using $X_1 = e^{At_4}X_4 + \mathscr{A}(t_4)F_1$. Go to step 1.

The expressions of $\mathscr{A}(t)$ and $\mathscr{B}(t)$ are defined in Appendix C. First, the travelling time t is determined by solving a non-linear equation $f(t) = 0$, where the explicit analytical expression of $f(t)$ can be found in reference [12]. This equation can be solved by any standard procedure such as bisection or Newton–Raphson method. Then, the new state X_i ($i = 1, 2, 3, 4$) are computed from a known matrix by a known vector multiplications. For example, in step 1, once the travelling time t_1 is determined, the new state vector X_2 can be updated from X_1 according to $X_2 = e^{Bt_1}X_1 + \mathscr{B}(t_1)F_2$. Recall that X_1 and F_2 are vectors, and from Appendix C, $e^{Bt_1} = P\bar{J}_B P^{-1}$ and $\mathscr{B}(t_1) = Q\bar{B}Q^{-1}$, where P, $\bar{J}_B$, $\bar{B}$ and Q are known matrices whose elements are defined in Appendix C. Hence, X_2 is determined by performing linear algebraic operations. If no positive solution for $f(t) = 0$ can be found in any of the steps discussed above, the motion either diverges if the linear system has at least one eigenvalue with a positive real part, or it converges to the equilibrium in that region if the real parts of all eigenvalues of the linear system are negative. If the values of the switching points or the amplitudes of α become unbounded, then the motion is divergent.

3.2. FORMULATION 2

If only the steady state solution of an aeroelastic model is of interest, the following alternative formulation is proposed so that the travelling times and the switching points of an LCO can be determined directly without going through the transient state. However, we must first assume the specified type of the investigated motion. For example, for a period-one LCO, the four switching points are defined by

$$X_1 = \begin{pmatrix} \alpha_f \\ s_1 \end{pmatrix}, \quad X_2 = \begin{pmatrix} \alpha_f + \delta \\ s_2 \end{pmatrix}, \quad X_3 = \begin{pmatrix} \alpha_f + \delta \\ s_3 \end{pmatrix}, \quad X_4 = \begin{pmatrix} \alpha_f \\ s_4 \end{pmatrix},$$

where s_1, s_2, s_3 and s_4 are seven-dimensional variable vectors representing the switching points in the subspace $\{X \in R^8 | x_1 = \alpha_f\}$ or $\{X \in R^8 | x_1 = \alpha_f + \delta\}$. Let t_i ($i = 1, 2, 3, 4$) denote the corresponding travelling times. Then t_i and s_i ($i = 1, 2, 3, 4$) can be determined by solving the following system of non-linear equations

$$X_2 = e^{Bt_1}X_1 + \mathscr{B}(t_1)F_2, \qquad X_3 = e^{At_2}X_2 + \mathscr{A}(t_2)F_3,$$

$$X_4 = e^{Bt_3}X_3 + \mathscr{B}(t_3)F_2, \qquad X_1 = e^{At_4}X_4 + \mathscr{A}(t_4)F_1. \tag{4}$$

Note that equation (4) is 32-dimensional since X_i ($i = 1, 2, 3, 4$) are eight-dimensional vectors. The period of this period-one LCO is given by the sum of the total travelling time $T = \sum_{i=1}^{4} t_i$, and the frequency f is calculated by $f = 1/T$. The amplitudes α_{max} and α_{min} are given by

$$\begin{aligned}
&\text{solve } \{e^{At_u}X_2 + \mathscr{A}(t_u)F_3\}|_{(2)} = 0 \text{ for } t_u,\\
&\text{set } \alpha_{max} = \{e^{At_u}X_2 + \mathscr{A}(t_u)F_3\}|_{(1)},\\
&\text{solve } \{e^{At_l}X_4 + \mathscr{A}(t_l)F_1\}|_{(2)} = 0 \text{ for } t_l,\\
&\text{set } \alpha_{min} = \{e^{At_l}X_4 + \mathscr{A}(t_l)F_1\}|_{(1)},
\end{aligned} \tag{5}$$

where X_2 and X_4 are solutions to equation (4).

To determine the frequency of an LCO, only the values of t_i ($i = 1, 2, 3, 4$) are of interest. With some algebra, the 32-dimensional non-linear equations system equation (4) can be further reduced to a four-dimensional system with respect to t_i ($i = 1, 2, 3, 4$).

$$\begin{aligned}
\alpha_f &= \{H_1(t_1, t_2, t_3, t_4)G_1(t_1, t_2, t_3, t_4)\}|_{(1)},\\
\alpha_f + \delta &= \{H_2(t_1, t_2, t_3, t_4)G_2(t_1, t_2, t_3, t_4)\}|_{(1)},\\
\alpha_f + \delta &= \{H_3(t_1, t_2, t_3, t_4)G_3(t_1, t_2, t_3, t_4)\}|_{(1)},\\
\alpha_f &= \{H_4(t_1, t_2, t_3, t_4)G_4(t_1, t_2, t_3, t_4)\}|_{(1)},
\end{aligned} \tag{6}$$

where H_i ($i = 1, 2, 3, 4$) are the 8×8 matrix functions of t_i ($i = 1, 2, 3, 4$), and G_i ($i = 1, 2, 3, 4$) are 8×1 vector functions of t_i ($i = 1, 2, 3, 4$). The expressions for H_i and G_i are defined in Appendix D. The frequency of the period-one LCO motion can then be determined by $f = 1/\sum_{i=1}^{4} t_i$, and the four switching points are given by $X_i = H_i(t_1, t_2, t_3, t_4)G_i(t_1, t_2, t_3, t_4)$ with $i = 1, 2, 3, 4$. The amplitudes α_{max} and α_{min} are given by equation (5).

For a period-one LCO with harmonics, assuming that the small loop in the state space covers regions R_1 and R_2, there exist six switching points instead of four as in the simple period-one motion. By adding two more switching points,

$$X_5 = \begin{pmatrix} \alpha_f \\ s_5 \end{pmatrix} \quad \text{and} \quad X_6 = \begin{pmatrix} \alpha_f \\ s_6 \end{pmatrix},$$

where s_5 and s_6 are seven-dimensional vectors representing the switching points in the subspace $\{X \in R^8 | x_1 = \alpha_f\}$. Equations (4) are then rewritten as

$$\begin{aligned}
X_2 &= e^{Bt_1}X_1 + \mathscr{B}(t_1)F_2, \qquad X_3 = e^{At_2}X_2 + \mathscr{A}(t_2)F_3,\\
X_4 &= e^{Bt_3}X_3 + \mathscr{B}(t_3)F_2, \qquad X_5 = e^{At_4}X_4 + \mathscr{A}(t_4)F_1,\\
X_6 &= e^{Bt_5}X_5 + \mathscr{B}(t_5)F_2, \qquad X_1 = e^{At_6}X_6 + \mathscr{A}(t_6)F_1.
\end{aligned} \tag{7}$$

Consequently, the frequency is given by $f = 1/\sum_{i=1}^{6} t_i$. Since the motion contains four values of amplitude for α when $\alpha' = 0$, the following additional formulas:

$$\text{solve } \{e^{At_m} X_5^1 + \mathscr{B}(t_m) F_2\}|_{(2)} = 0 \text{ for } t_m,$$

$$\alpha_{max} = \{e^{At_m} X_5^1 + \mathscr{B}(t_m) F_2\}|_{(1)},$$

$$\text{solve } \{e^{At_n} X_6^1 + \mathscr{A}(t_n) F_1\}|_{(2)} = 0 \text{ for } t_n,$$

$$\alpha_{min} = \{e^{At_n} X_6^1 + \mathscr{A}(t_n) F_1\}|_{(1)} \tag{8}$$

are included into equation (5) to compute the LCO amplitudes.

Generally speaking, for a period-n LCO or a period-n LCO with harmonics, equations (4) and (5) or equations (7) and (8) must be modified to determine the corresponding travelling times and the amplitudes.

Although Formulation 1 starts with a given set of initial conditions, it is not a time-integration scheme since the solution to each linear subsystem is determined analytically. The formulation given in section 3.1 is capable of detecting any type of steady state motion including convergent, divergent, period-n, period-n with harmonics, and chaotic motions. Under the same system parameters, starting from different initial conditions, the trajectory may converge to different LCOs, which indicates the coexistence of the LCOs of the original system (2).

When Formulation 2 is applied, only the steady state behavior is detected since no information with respect to the transients is used. This is very efficient if only the steady state solution is of interest. However, the formulations given in equations (4) and (5) (or equations (7) and (8)) are valid only for detecting a period-one LCO (or a period-one LCO with harmonics). For other types of motion, the formulation has to be modified correspondingly. Note that only the positive solutions of t_i ($i = 1, 2, 3, 4$) to equation (4) (or equation (7)) are valid since the variables t_i ($i = 1, 2, 3, 4$) represent the travelling times. Also note that one valid solution of equation (4) (or equation (7)) corresponds to one period-one LCO (or one period-one LCO with harmonics) of the original system (2). However, there may be other valid solutions to equation (4) (or equation (7)), indicating the coexistence of period-one LCOs (or of period-one LCOs with harmonics). Furthermore, under the same system parameters, we may have valid solutions to equation (4) (or equation (7)) and to some other similar non-linear equation systems corresponding to other types of LCOs. However, Formulation 2 cannot be used to predict convergent, divergent or chaotic motions.

4. RESULTS AND DISCUSSIONS

To demonstrate the effectiveness of the point transformation method, Formulations 1 and 2 are applied to a freeplay model. The system parameters under consideration are $\mu = 100$, $a_h = -1/2$, $x_\alpha = 1/4$, $\zeta_\xi = \zeta_\alpha = 0$, $r_\alpha = 0{\cdot}5$ and $\bar{\omega} = 0{\cdot}2$. These system parameters are chosen from Price *et al.* [3]. The procedures discussed in the previous section do not depend on the choice of parameters. The non-linear restoring force $M(x_1)$ is given by equation (3) with $M_0 = 0$, $\delta = 0{\cdot}5^\circ$, $M_f = 0$, and $\alpha_f = 0{\cdot}25^\circ$, and the plunge is linear with $G(x_3) = x_3$.

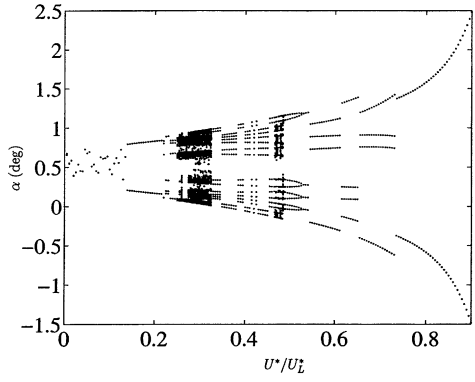

Figure 6. Bifurcation diagram for $\alpha(0) = 3^\circ$ and $\alpha'(0) = \xi(0) = \xi'(0) = 0$.

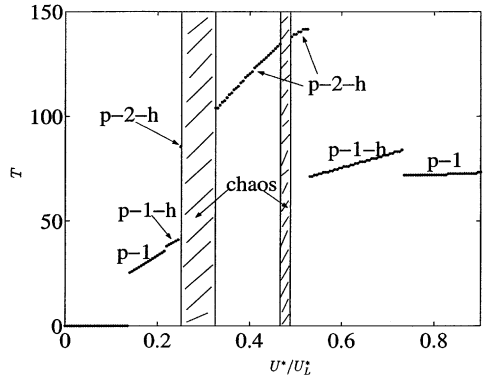

Figure 7. Period diagram for $\alpha(0) = 3^\circ$ and $\alpha'(0) = \xi(0) = \xi'(0) = 0$.

The linear flutter speed $U_L^* = 6{\cdot}2851$ is determined by solving the aeroelastic system for $M_0 = \delta = \alpha_f = 0$. For $U^* > U_L^*$, some of the eigenvalues in regions R_1, R_2 and R_3 have positive real parts. Thus, the solution is divergent. As U^* decreases below U_L^*, the real parts of all eigenvalues of systems in R_1 and R_3 are negative, but some eigenvalues of the system in R_2 may have positive real parts. Hence, for $U^* < U_L^*$, the aeroelastic system admits various non-linear behaviors. When all eigenvalues of the system in region R_2 have negative real parts, damped oscillation results, and the solution converges to its equilibrium point after the transients die out. However, when some of the eigenvalues of the system in R_2 have positive real parts, the solution could become a fixed point, a limit cycle oscillation or a chaotic motion.

Numerous simulations over a wide range of velocities $0 < U^*/U_L^* < 1$ have been performed using Formulation 1. Note that the non-linear aeroelastic response for a freeplay model depends strongly on the initial conditions. In this study, the value of $\alpha(0)$ is selected to be in the range $\pm 5^\circ$ so that the steady state solution for pitch and plunge are small enough for linear aerodynamics to be valid. For the results presented in this section, we report those using a non-zero value for $x_1(0)$ (i.e., $\alpha(0)$), and other values $x_i(0)$ for $i = 2, 3, \ldots, 8$ are set to zero. To illustrate the complex non-linear system behaviors, we display a bifurcation diagram and a period diagram in Figures 6 and 7. The results reported are obtained using Formulation 1, and they correspond to the choice of $\alpha(0) = 3^\circ$. In these two figures, the

TABLE 1

Cases studies for freeplay

Case	U^*/U_L^*	Type of motion	T	α_{max} (deg)	α_{min} (deg)
1	0·20	p-1	33·4464	0·8311	0·1689
2	0·22	p-1-h	37·9893	0·8872	0·1653
3	0·2510	p-2-h	83·5829	0·9063	0·1567
4	0·3	Chaotic			

horizontal axis is the bifurcation parameter U^*/U_L^*. The vertical axis is the maximum and minimum values of the pitch angle when $\alpha' = 0$ in Figure 6. In Figure 7, we present the values of the LCO's period, and the classification of the steady state solution is also described where p-n denotes a period-n LCO and p-n-h denotes a period-n LCO with harmonics.

For $0 < U^*/U_L^* \leqslant 0{\cdot}13$, a single point is shown in the bifurcation diagram, which indicates that the solution converges to an equilibrium point. Since zero travelling time is determined by Formulation 1, this corresponds to a zero value for the period shown in Figure 7. For example, when $U^* = 0{\cdot}07U_L^*$, no positive solution for the travelling time can be found in Step 3 of Formulation 1. The zero time implies that the solution will not pass through the regions R_1 and R_3. Since the real parts of all eigenvalues of the system in R_2 are negative, the solution converges to the equilibrium point in R_2. For $0{\cdot}14 \leqslant U^*/U_L^* \leqslant 0{\cdot}215$, two amplitudes of α corresponding to the maximum and minimum of pitch when $\alpha' = 0$ are shown in Figure 6. This indicates that the solution is an LCO with period-one. It has one frequency with the period given in Figure 7. For $0{\cdot}216 \leqslant U^*/U_L^* \leqslant 0{\cdot}245$, four amplitudes of α and $\alpha' = 0$ are shown in Figure 6, and four switching points are detected by both formulations. Thus, the solution is a period-one LCO with harmonics, and the period, which is the same amount as the total travelling time, is shown in the corresponding period diagram. Note that there exists a small jump in the value of the LCO period when the solutions change from simple period-one to period-one with harmonics. Increasing U^* slightly to $U^* = 0{\cdot}25U_L^*$, we observe a large jump in the period and eight values of α when $\alpha' = 0$ for the steady state. Note that the period is almost double, indicating the appearance of a period-doubling phenomenon. The solution becomes a period-two LCO with harmonics. The type of motion remains unchanged for $0{\cdot}25 \leqslant U^*/U_L^* \leqslant 0{\cdot}529$ except for two intervals when $0{\cdot}252 \leqslant U^*/U_L^* < 0{\cdot}325$ and $0{\cdot}466 \leqslant U^*/U_L^* \leqslant 0{\cdot}488$, where the solution becomes chaotic as shown in Figure 6. A large number of amplitudes of α when $\alpha' = 0$ are detected in the chaotic regions, and they appear to lie along a vertical line in the bifurcation diagram. As U^* increases to $0{\cdot}53U_L^*$, a large drop with a factor of two in the period occurs, and the solutions change from period-two with harmonics to period-one with harmonics. A further small reduction in amplitude for pitch appears when $U^*/U_L^* = 0{\cdot}732$, and the solution becomes a simple period-one LCO.

In order to illustrate the equivalence of both Formulations 1 and 2, four typical cases are selected for a more detailed examination. The results corresponding to the choice of initial condition $\alpha(0) = 3^\circ$ are presented in Table 1 and in Figures 8–11. In Table 1, T represents the period, and α_{max} and α_{min} denote the absolute maximum and minimum values of pitch. The solutions obtained from both formulations are essentially identical, and they are in good agreement with the numerical solution obtained by the Runge–Kutta time-integration scheme. The results obtained from the point transformation method are denoted by filled circles in the figures, and the numerical solutions from the time-integration scheme are

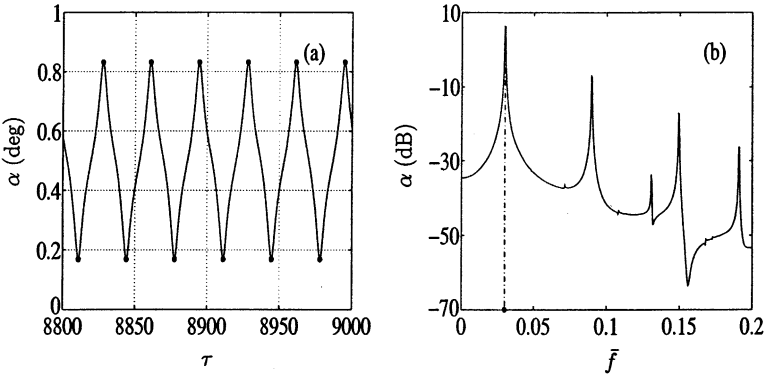

Figure 8. (a) The time history and (b) power spectral density (PSD) plot of pitch motion for Case 1 in Table 1. ——, Runge–Kutta time-integration result; ●, point transformation result.

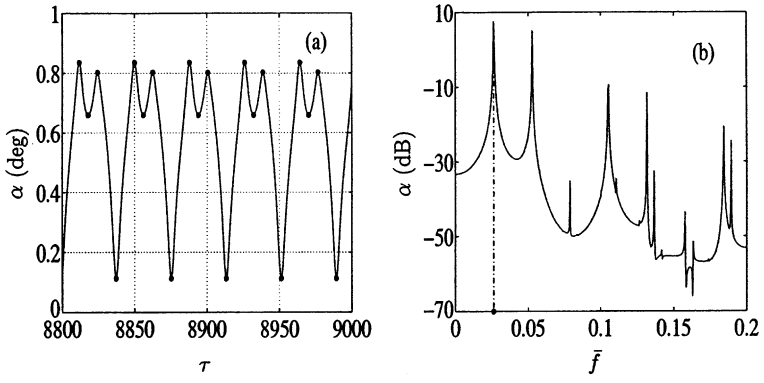

Figure 9. (a) The time history and (b) PSD plot of pitch motion for Case 2 in Table 1. ——, Runge–Kutta time-integration result; ●, point transformation result.

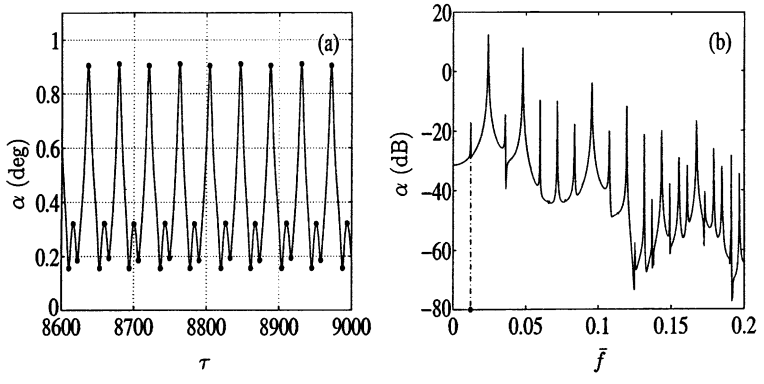

Figure 10. (a) The time history and (b) PSD plot of pitch motion for Case 3 in Table 1. ——, Runge–Kutta time-integration result; ●, point transformation result.

illustrated by solid lines. It should be noted that the time step is usually chosen so that the time-integration method provided a stable numerical solution. Since for an aeroelastic system with freeplay, some of the eigenvalues of the system in region R_2 may have positive real parts, it is difficult to perform the standard stability analysis. In numerical simulations,

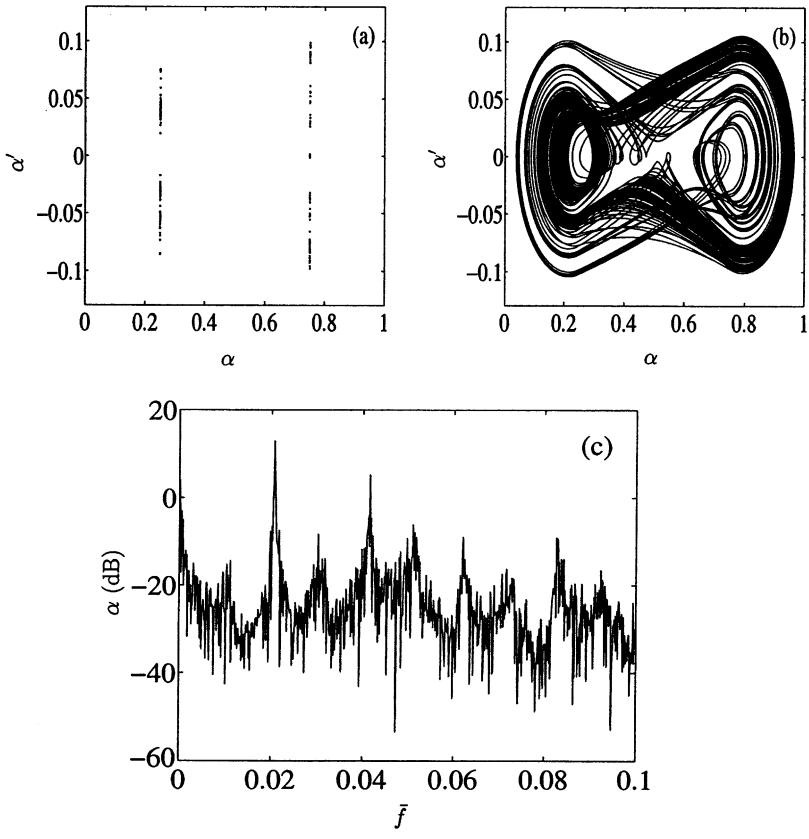

Figure 11. Chaotic motion of Case 4 in Table 1: (a) the switching points by using point transformation method; (b) the phase path by using Runge–Kutta time-integration; (c) the PSD plot.

the time step Δt is chosen to be sufficiently small in order to ensure that a good accuracy is achieved. Here, Δt can only be selected numerically when the solution computed by Δt is essentially the same as those obtained using $\Delta t/2$. We found that the choice of Δt depends strongly on the bifurcation parameter. For the freeplay model presented in Table 1, the result by using $\Delta t = 0{\cdot}3$ is found to be a good numerical solution for $U^* = 0{\cdot}2U_L^*$. As U^* increases to $0{\cdot}25U_L^*$, much smaller time step $\Delta t = 0{\cdot}0125$ must be used to obtain an accurate solution. The choice of Δt becomes more critical as the solution approaches chaos. Hence, solving an aeroelastic system using a numerical method becomes very time consuming, because a large number of computing steps per cycle is required especially when U^* nears the chaotic regions. Moreover, the appropriate value for Δt can be determined only through a sequence of numerical computations using Δt, $\Delta t/2$, $\Delta t/4$, ..., etc.

For Case 1, using Formulation 1 starting with $\alpha(0) = 3^\circ$, an LCO is detected after eight cycles. Four switching points and four travelling times are recorded, and they are similar to those displayed in Figure 3(b). Since two amplitudes of α corresponding to $\alpha' = 0$ are determined (Figure 8), we conclude that the LCO is period-one with the frequency given by the non-dimensional $f = 1/T = 0{\cdot}0299$. The predicted frequency is in excellent agreement with that determined from the power spectral density (PSD) plot based on the time history of the numerical solution (Figure 8(b)). When Formulation 2 is applied, the same amplitudes and frequency are obtained directly without the transient stage. As U^* increases to $0{\cdot}22U_L^*$, six switching points and travelling times are recorded, and they are similar to those shown

TABLE 2

Coexistence of limit cycle oscillations

Case	U^*/U_L^*	$x_1(0)$ (deg)	Type of motion	T	α_{max} (deg)	α_{min} (deg)
1	0·2161	0·3	p-1-h	37·5344	0·8341	0·1149
2	0·2161	3	p-1	35·6384	0·8403	0·1597
3	0·22	− 3	p-1-h	37·9893	0·8347	0·1128
4	0·22	3	p-1-h	37·9893	0·8872	0·1653
5	0·7	− 0·5	p-1-h	81·9875	1·5179	0·2451
6	0·7	− 5	p-1	72·05	1·2973	−0·2973

in Figure 4(a). The existence of a smaller loop covering regions R_1 and R_2 indicates that the LCO has harmonics. Four amplitudes of α when $\alpha' = 0$ are detected, and they are in good agreement with the numerical solution (Figure 9(a)). The frequency $f = 1/T = 0{\cdot}0263$ agrees well with the first dominant frequency reported from the PSD plot shown in Figure 9(b). The point transformation method confirms the existence of the harmonic components, but it is unable to predict the value of the harmonics which appears at $2f = 0{\cdot}0526$ as shown in the PSD plot.

For Case 3, the period $T = 83{\cdot}58$, which is almost double the period $T = 37{\cdot}98$ reported for Case 2. Both Formulations 1 and 2 indicate 12 switching points and eight amplitudes of α when $\alpha' = 0$. Moreover, the switching points displayed in the phase plane are similar to those shown in Figure 5(b), where the complete loop covers the entire region twice, and it also contains two smaller loops covering regions R_1 and R_2. Hence, the resulting LCO is of period-two with harmonics. Figure 10 shows the pitch amplitudes corresponding to $\alpha' = 0$ and the predicted frequency of the LCO.

When $U^* = 0{\cdot}3U_L^*$, the values of switching points, travelling times, and the amplitudes of α obtained using Formulation 1 do not settle down to a repeated sequence even after a sufficiently long time when $\tau > 15\,000$. The switching points appear to be on a vertical line in the phase space of α–α' as shown in Figure 11(a). The amplitudes of α when $\alpha' = 0$ also lie on a vertical line in the bifurcation diagram shown in Figure 6. The suggests that the motion is chaotic. The chaos is confirmed from a phase trajectory of α–α' (Figure 11(b)) resulting from the numerical time-integration scheme, and a typical "two-well potential" trajectory is observed. It is also worthwhile to note that the locations of the two inner loops are near the subspaces corresponding to $\alpha = 0{\cdot}25$ and $0{\cdot}75^\circ$. The PSD spectrum (Figure 11(c)) from the numerical solution also confirms the existence of broadband frequency components, an indication of chaos. The particular case was also investigated by Price *et al.* [3], and they concluded that the motion is indeed chaotic.

One of the important features of the freeplay model is that the aeroelastic system admits the coexistence of stable LCOs. Table 2 reports the case with the speed ratio $U^*/U_L^* = 0{\cdot}2161$, $0{\cdot}22$ and $0{\cdot}7$. Starting with various initial conditions for $\alpha(0)$, different LCOs are predicted by Formulation 1. For example, for $U^* = 0{\cdot}2161U_L^*$ and $\alpha(0) = 0{\cdot}3^\circ$, the LCO converges to a period-one LCO with harmonics, where the frequency is given by $f = 0{\cdot}0266$. Changing the initial condition to $\alpha(0) = 3^\circ$, the solution becomes a simple period-one LCO, and the frequency is given by $f = 0{\cdot}0281$. For $U^* = 0{\cdot}22U_L^*$, the solutions corresponding to the initial conditions $\alpha(0) = \pm 3^\circ$ are of the same type, namely period-one LCO with harmonics. Although the periods are identical, the amplitudes of α when $\alpha' = 0$ are different. The point transformation method confirms that the locations of the six switching points are actually different, and they are similar to those shown in Figure 4(a)

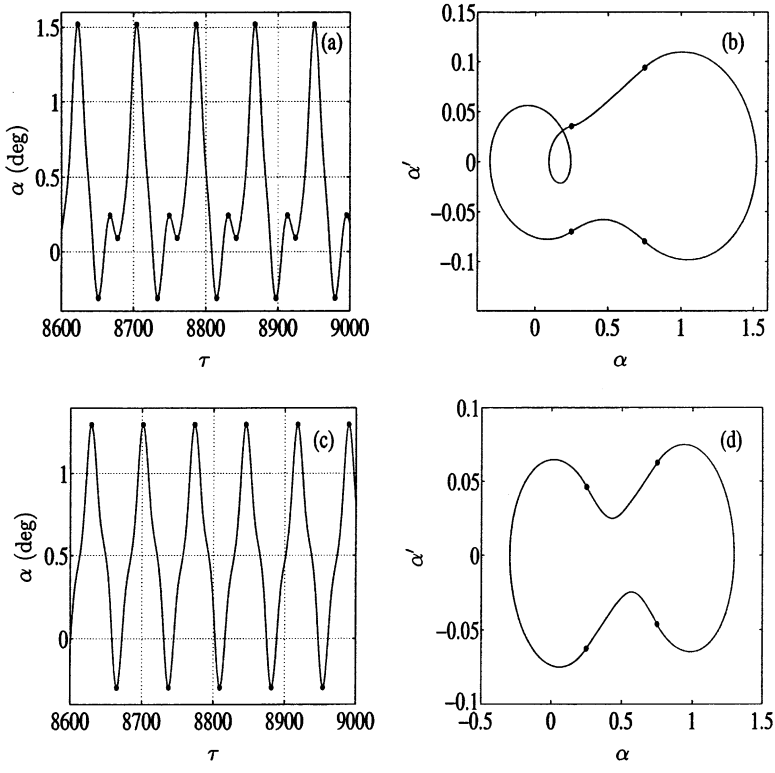

Figure 12. The time histories and phase paths, (a) and (b) for Case 5, (c) and (d) for Case 6 in Table 2. ——, Runge–Kutta time-integration result; ●, point transformation result.

and 4(b). Note that the smaller loop covers regions R_1 and R_2 for Case 3 and regions R_2 and R_3 for Case 4. For $U^* = 0{\cdot}7U_L^*$, four switching points are found by the point transformation method when $\alpha(0) = -0{\cdot}5^\circ$ and $-5{\cdot}0^\circ$. However, the number of amplitudes of α when $\alpha' = 0$ are found to be four and two as shown in Figure 12(a) and 12(c), corresponding to the above initial conditions. This gives an indication of the existence of harmonic components for Case 5. The phase trajectory constructed from the numerical time-integration solution confirms the existence of a smaller loop as shown in Figure 12(b) and 12(d). However, since the smaller loop exists only in the region R_1, no extra switching point is found in the point transformation method.

Although no explicit information concerning the initial condition is required in Formulation 2, the coexistence of stable LCOs can be determined by solving different sets of non-linear equations or by changing the initial guess values to solve the same set of non-linear equations. For $U^*/U_L^* = 0{\cdot}2161$, solving equations (4) or (6) gives the LCO in Case 2, and the solution of equation (7) leads to the LCO in Case 1. Similarly, when $U^*/U_L^* = 0{\cdot}22$, solving equation (7) gives the LCO in Case 3. In order to determine the motion type for Case 4, a different set of non-linear equations must be developed, since the switching points are now in a different sequence. Cases 5 and 6 correspond to two different types of LCOs, but both have four switching points, X_1, X_2, X_3 and X_4. The switching points and travelling times are determined by solving the same non-linear equations (4) in Formulation 2 but with different initial guess values. Table 3 reports the values of the initial guess which are used for solving equation (4) in which other initial starting values s_i ($i = 1, 2,$

TABLE 3

Results of Formulation 2 for Cases 5 and 6 in Table 2

	t_1	t_2	t_3	t_4
Initial guess	10	30	10	30
Final solution	8·85644138	20·57834338	7·86033041	44·68989101
Initial guess	5	20	10	20
Final solution	20·18151269	21·03447205	10·70421369	22·42792629

3, 4) are set to zero. The corresponding solution for t_1, t_2, t_3 and t_4 are presented in Table 3. These results confirm the coexistence of two stable LCOs with two different periods, namely $T = 82$ and 72 for Cases 5 and 6 respectively.

5. CONCLUSIONS

A mathematical technique based on the point transformation method has been developed to investigate the dynamic response of a self-excited two-d.o.f. aeroelastic system with structural non-linearity represented by a freeplay stiffness. The method provides an accurate prediction since the switching points where the changes in linear subdomains occur are located exactly, and the solution in each subdomain is determined analytically. The formulations are developed, and they have been applied to investigate the non-linear aeroelastic behavior of a freeplay model. The results of the present study show that both formulations can accurately predict the frequency and amplitude of limit cycle oscillations. Moreover, the formulations are also capable of detecting complex non-linear behavior such as periodic motions with harmonics, period doubling, chaotic motions and the coexistence of stable limit cycles. Formulation 2 is particularly attractive since it can detect the presence of a particular type of LCO directly without considering the transients. From the illustrative examples presented in this paper, it is clearly demonstrated that analytic predictions are in excellent agreement with those resulting from a numerical time-integration scheme. The point transformation formulations are developed for an aeroelastic system with a structural non-linearity in the pitch d.o.f. However, the analysis can readily be extended to include non-linearities in both d.o.f.

ACKNOWLEDGMENTS

The authors would like to acknowledge the support received from the Natural Sciences and Engineering Research Council of Canada.

REFERENCES

1. H. ALIGHANBARI and S. J. PRICE 1996 *Nonlinear Dynamics* **10**, 381–400. The post- Hopf-bifurcation response of an airfoil in incompressible two-dimensional flow.
2. E. J. BREITBACH 1980 *NASA TP* 1620. Flutter analysis of an airplane with multiple structural nonlinearities in the control system.
3. S. J. PRICE, H. ALIGHANBARI and B. H. K. LEE 1995 *Journal of Fluids and Structures* **9**, 175–193. The aeroelastic response of a two-dimensional airfoil with bilinear and cubic structural nonlinearities.

4. S. J. PRICE, B. H. K. LEE and H. ALIGHANBARI 1994 *Journal of Aircraft* **31**, 1395–1401. Post instability behavior of a two-dimensional airfoil with a structural nonlinearity.
5. S. F. SHEN 1959 *Journal of Aerospace Science* **26**, 25–32. An approximate analysis of nonlinear flutter problems.
6. B. H. K. LEE, S. J. PRICE and Y. S. WONG 1999 *Progress in Aerospace Sciences* **35**, 205–334. Nonlinear aeroelastic analysis of airfoils: bifurcation and chaos.
7. L. LIU, Y. S. WONG and B. H. K. LEE 2000 *Journal of Sound and Vibration* **234**, 641–659. Application of the centre manifold theory in nonlinear aeroelasticity.
8. L. LIU, Y. S. WONG and B. H. K. LEE 2002 *Journal of Sound and Vibration* **253**, Nonlinear aeroelastic analysis using the point transformation method, Part 2: hysteresis model.
9. B. H. K. LEE and J. DESROCHERS 1987 *Aeronautical Report LR*-618, *NRC No*. 27833, *National Research Council of Canada*. Flutter analysis of a two-dimensional airfoil containing structural nonlinearities.
10. M. D. CONNER, D. M. TANG, E. H. DOWELL and L. N. VIRGIN 1997 *Journal of Fluids and Structures* **11**, 89–109. Nonlinear behavior of a typical airfoil section with control surface freeplay: a numerical and experimental study.
11. D. M. TANG and E. H. DOWELL 1992 *Journal of Aircraft* **29**, 953–960. Flutter and stall response of a helicoptor blade with structural nonliearity.
12. L. LIU 2001 *Ph. D. Dissertation*, *University of Alberta*, *Edmonton*, *AB*, *Canada*. Mathematical analysis of nonlinear aeroelasticity.
13. W. B. LIN and W. H. CHENG 1993 *Journal of the Chinese Society of Mechanical Engineers* **14**, 446–466. Nonlinear flutter of loaded lifting surfaces (I) and (II).
14. L. LIU, Y. S. WONG and B. H. K. LEE 2002 *International Journal of Numerical Methods in Engineering*, to be published. Error analysis of Runge–Kutta's discretizations of certain types of dynamic systems.
15. A. A. ANDRONOV, A. A. VITT and S. E. KHAIKIN 1966 *Theory of Oscillators*. Reading, Massachusetts: Addison–Wesley Publishing Company Inc.
16. Y. C. FUNG 1955 *An Introduction to the Theory of Aeroelasticity*. New York: Dover Publications Inc.

APPENDIX A: DEFINITIONS OF COEFFICIENTS

$$a_{21} = j(-d_5c_0 + c_5d_0), \quad a_{41} = j(d_5c_1 - c_5d_1),$$

$$a_{22} = j(-d_3c_0 + c_3d_0), \quad a_{42} = j(d_3c_1 - c_3d_1),$$

$$a_{23} = j(-d_4c_0 + c_4d_0), \quad a_{43} = j(d_4c_1 - c_4d_1),$$

$$a_{24} = j(-d_2c_0 + c_2d_0), \quad a_{44} = j(d_2c_1 - c_2d_1),$$

$$a_{25} = j(-d_6c_0 + c_6d_0), \quad a_{45} = j(d_6c_1 - c_6d_1),$$

$$a_{26} = j(-d_7c_0 + c_7d_0), \quad a_{46} = j(d_7c_1 - c_7d_1),$$

$$a_{27} = j(-d_8c_0 + c_8d_0), \quad a_{47} = j(d_8c_1 - c_8d_1),$$

$$a_{28} = j(-d_9c_0 + c_9d_0), \quad a_{48} = j(d_9c_1 - c_9d_1),$$

where j, c_i ($i = 0, 1, 2, \ldots, 9$) and d_i ($i = 0, 1, 2, \ldots, 9$) are defined as

$$j = \frac{1}{c_0d_1 - c_1d_0},$$

$$c_0 = 1 + \frac{1}{\mu}, \quad c_1 = x_\alpha - \frac{a_h}{\mu},$$

$$c_2 = \frac{2}{\mu}(1 - \psi_1 - \psi_2), \quad c_3 = \frac{1}{\mu}(1 + (1 - 2a_h)(1 - \psi_1 - \psi_2)),$$

$$c_4 = \frac{2}{\mu}(\varepsilon_1\psi_1 + \varepsilon_2\psi_2), \quad c_5 = \frac{2}{\mu}\left(1 - \psi_1 - \psi_2 + \left(\frac{1}{2} - a_h\right)(\varepsilon_1\psi_1 + \varepsilon_2\psi_2)\right),$$

$$c_6 = \frac{2}{\mu}\varepsilon_1\psi_1\left(1 - \varepsilon_1\left(\frac{1}{2} - a_h\right)\right), \quad c_7 = \frac{2}{\mu}\varepsilon_2\psi_2\left(1 - \varepsilon_2\left(\frac{1}{2} - a_h\right)\right),$$

$$c_8 = -\frac{2}{\mu}\varepsilon_1^2\psi_1, \quad c_9 = -\frac{2}{\mu}\varepsilon_2^2\psi_2,$$

$$d_0 = \frac{x_\alpha}{r_\alpha^2} - \frac{a_h}{\mu r_\alpha^2}, \quad d_1 = 1 + \frac{1 + 8a_h^2}{8\mu r_\alpha^2},$$

$$d_2 = -\frac{1 + 2a_h}{\mu r_\alpha^2}(1 - \psi_1 - \psi_2),$$

$$d_3 = \frac{1 - 2a_h}{2\mu r_\alpha^2} - \frac{(1 + 2a_h)(1 - 2a_h)(1 - \psi_1 - \psi_2)}{2\mu r_\alpha^2},$$

$$d_4 = -\frac{1 + 2a_h}{\mu r_\alpha^2}(\varepsilon_1\psi_1 + \varepsilon_2\psi_2),$$

$$d_5 = -\frac{1 + 2a_h}{\mu r_\alpha^2}(1 - \psi_1 - \psi_2) - \frac{(1 + 2a_h)(1 - 2a_h)(\psi_1\varepsilon_1 - \psi_2\varepsilon_2)}{2\mu r_\alpha^2},$$

$$d_6 = -\frac{(1 + 2a_h)\psi_1\varepsilon_1}{\mu r_\alpha^2}\left(1 - \varepsilon_1\left(\frac{1}{2} - a_h\right)\right),$$

$$d_7 = -\frac{(1 + 2a_h)\psi_2\varepsilon_2}{\mu r_\alpha^2}\left(1 - \varepsilon_2\left(\frac{1}{2} - a_h\right)\right),$$

$$d_8 = \frac{(1 + 2a_h)\psi_1\varepsilon_1^2}{\mu r_\alpha^2}, \quad d_9 = \frac{(1 + 2a_h)\psi_2\varepsilon_2^2}{\mu r_\alpha^2}.$$

APPENDIX B: DEFINITIONS OF MATRICES AND VECTORS

$$A_1 = \begin{pmatrix} 0 & 1 & 0 & 0 \\ a_{21} - jc_0\left(\frac{1}{U^*}\right)^2 & a_{22} & a_{23} + jd_0\beta\left(\frac{\bar{\omega}}{U^*}\right)^2 & a_{24} \\ 0 & 0 & 0 & 1 \\ a_{41} + jc_1\left(\frac{1}{U^*}\right)^2 & a_{42} & a_{43} - jd_1\beta\left(\frac{\bar{\omega}}{U^*}\right)^2 & a_{44} \end{pmatrix},$$

$$A_2 = \begin{pmatrix} 0 & 0 & 0 & 0 \\ a_{25} & a_{26} & a_{27} & a_{28} \\ 0 & 0 & 0 & 0 \\ a_{45} & a_{46} & a_{47} & a_{48} \end{pmatrix}, \quad A_3 = \begin{pmatrix} 1 & 0 & 0 & 0 \\ 1 & 0 & 0 & 0 \\ 0 & 0 & 1 & 0 \\ 0 & 0 & 1 & 0 \end{pmatrix}, \quad A_4 = \begin{pmatrix} -\varepsilon_1 & 0 & 0 & 0 \\ 0 & -\varepsilon_2 & 0 & 0 \\ 0 & 0 & -\varepsilon_1 & 0 \\ 0 & 0 & 0 & -\varepsilon_2 \end{pmatrix},$$

$$B_1 = \begin{pmatrix} 0 & 1 & 0 & 0 \\ a_{21} - jc_0M_f\left(\frac{1}{U^*}\right)^2 & a_{22} & a_{23} + jd_0\beta\left(\frac{\bar{\omega}}{U^*}\right)^2 & a_{24} \\ 0 & 0 & 0 & 1 \\ a_{41} + jc_1M_f\left(\frac{1}{U^*}\right)^2 & a_{42} & a_{43} - jd_1\beta\left(\frac{\bar{\omega}}{U^*}\right)^2 & a_{44} \end{pmatrix}, \qquad F = \begin{pmatrix} 0 \\ -jc_0\left(\frac{1}{U^*}\right)^2 \\ 0 \\ jc_1\left(\frac{1}{U^*}\right)^2 \\ 0 \\ 0 \\ 0 \\ 0 \end{pmatrix}.$$

APPENDIX C: COMPUTATION OF THE MATRICES

Let the matrices A and B be decomposed such that $A = PJ_AP^{-1}$ and $B = QJ_BQ^{-1}$, where J_A and J_B are the Jordan canonical forms of A and B:

$$J_A = \begin{pmatrix} a & b & 0 & 0 & 0 & 0 & 0 & 0 \\ -b & a & 0 & 0 & 0 & 0 & 0 & 0 \\ 0 & 0 & c & d & 0 & 0 & 0 & 0 \\ 0 & 0 & -d & c & 0 & 0 & 0 & 0 \\ 0 & 0 & 0 & 0 & \lambda_{a_1} & 0 & 0 & 0 \\ 0 & 0 & 0 & 0 & 0 & \lambda_{a_2} & 0 & 0 \\ 0 & 0 & 0 & 0 & 0 & 0 & \lambda_{a_3} & 0 \\ 0 & 0 & 0 & 0 & 0 & 0 & 0 & \lambda_{a_4} \end{pmatrix},$$

and

$$J_B = \begin{pmatrix} e & f & 0 & 0 & 0 & 0 & 0 & 0 \\ -f & e & 0 & 0 & 0 & 0 & 0 & 0 \\ 0 & 0 & \lambda_{b_1} & 0 & 0 & 0 & 0 & 0 \\ 0 & 0 & 0 & \lambda_{b_2} & 0 & 0 & 0 & 0 \\ 0 & 0 & 0 & 0 & \lambda_{b_3} & 0 & 0 & 0 \\ 0 & 0 & 0 & 0 & 0 & \lambda_{b_4} & 0 & 0 \\ 0 & 0 & 0 & 0 & 0 & 0 & \lambda_{b_5} & 0 \\ 0 & 0 & 0 & 0 & 0 & 0 & 0 & \lambda_{b_6} \end{pmatrix},$$

where $\{a \pm bi, c \pm di, \lambda_{a_1}, \lambda_{a_2}, \lambda_{a_3}, \lambda_{a_4}\}$ and $\{e \pm fi, \lambda_{b_1}, \lambda_{b_2}, \lambda_{b_3}, \lambda_{b_4}, \lambda_{b_5}, \lambda_{b_6}\}$ are eigenvalues of A and B respectively. The matrix $\mathscr{A}(t) = \int_0^t \mathrm{e}^{A(t-\tau)}\,\mathrm{d}\tau$ can be computed by $\mathscr{A}(t) = P\bar{A}P^{-1}$, where

$$\bar{A} = \begin{pmatrix} v(a,b,t) & s(a,b,t) & 0 & 0 & 0 & 0 & 0 & 0 \\ -s(a,b,t) & v(a,b,t) & 0 & 0 & 0 & 0 & 0 & 0 \\ 0 & 0 & v(c,d,t) & s(c,d,t) & 0 & 0 & 0 & 0 \\ 0 & 0 & -s(c,d,t) & v(c,d,t) & 0 & 0 & 0 & 0 \\ 0 & 0 & 0 & 0 & l(\lambda_{a_1},t) & 0 & 0 & 0 \\ 0 & 0 & 0 & 0 & 0 & l(\lambda_{a_2},t) & 0 & 0 \\ 0 & 0 & 0 & 0 & 0 & 0 & l(\lambda_{a_3},t) & 0 \\ 0 & 0 & 0 & 0 & 0 & 0 & 0 & l(\lambda_{a_4},t) \end{pmatrix}$$

and the matrix $\mathscr{B}(t) = \int_0^t \mathrm{e}^{B(t-\tau)}\,\mathrm{d}\tau$ can be computed by $\mathscr{B}(t) = Q\bar{B}Q^{-1}$, where

$$\bar{B} = \begin{pmatrix} v(e,f,t) & s(e,f,t) & 0 & 0 & 0 & 0 & 0 & 0 \\ -s(e,f,t) & v(e,f,t) & 0 & 0 & 0 & 0 & 0 & 0 \\ 0 & 0 & l(\lambda_{b_1},t) & 0 & 0 & 0 & 0 & 0 \\ 0 & 0 & 0 & l(\lambda_{b_2},t) & 0 & 0 & 0 & 0 \\ 0 & 0 & 0 & 0 & l(\lambda_{b_3},t) & 0 & 0 & 0 \\ 0 & 0 & 0 & 0 & 0 & l(\lambda_{b_4},t) & 0 & 0 \\ 0 & 0 & 0 & 0 & 0 & 0 & l(\lambda_{b_5},t) & 0 \\ 0 & 0 & 0 & 0 & 0 & 0 & 0 & l(\lambda_{b_6},t) \end{pmatrix},$$

and where the functions $v\colon R^3 \to R$, $s\colon R^3 \to R$, and $l\colon R^2 \to R$ are given by

$$v(a,b,t) = \int_0^t \mathrm{e}^{a(t-\tau)}\cos(b(t-\tau))\,\mathrm{d}\tau = \frac{-a + a\mathrm{e}^{at}\cos(bt) + b\mathrm{e}^{at}\sin(bt)}{a^2+b^2},$$

$$s(a,b,t)=\int_0^t \mathrm{e}^{a(t-\tau)}\sin(b(t-\tau))\,\mathrm{d}\tau=\frac{b-b\mathrm{e}^{at}\cos(bt)+a\mathrm{e}^{at}\sin(bt)}{a^2+b^2},$$

$$l(\lambda,t)=\int_0^t \mathrm{e}^{\lambda(t-\tau)}\,\mathrm{d}\tau=\begin{cases}\dfrac{\mathrm{e}^{\lambda t}-1}{\lambda}, & \lambda\neq 0,\\ t, & \lambda=0.\end{cases}$$

Also, $\mathrm{e}^{At}=P\bar{J}_AP^{-1}$ and $\mathrm{e}^{Bt}=Q\bar{J}_BQ^{-1}$, where

$$\bar{J}_A=\begin{pmatrix}
\mathrm{e}^{at}\cos(bt) & \mathrm{e}^{at}\sin(bt) & 0 & 0 & 0 & 0 & 0 & 0\\
-\mathrm{e}^{at}\sin(bt) & \mathrm{e}^{at}\cos(bt) & 0 & 0 & 0 & 0 & 0 & 0\\
0 & 0 & \mathrm{e}^{ct}\cos(\mathrm{d}t) & \mathrm{e}^{ct}\sin(\mathrm{d}t) & 0 & 0 & 0 & 0\\
0 & 0 & -\mathrm{e}^{ct}\sin(\mathrm{d}t) & \mathrm{e}^{ct}\cos(\mathrm{d}t) & 0 & 0 & 0 & 0\\
0 & 0 & 0 & 0 & \mathrm{e}^{\lambda_{a_1}t} & 0 & 0 & 0\\
0 & 0 & 0 & 0 & 0 & \mathrm{e}^{\lambda_{a_2}t} & 0 & 0\\
0 & 0 & 0 & 0 & 0 & 0 & \mathrm{e}^{\lambda_{a_3}t} & 0\\
0 & 0 & 0 & 0 & 0 & 0 & 0 & \mathrm{e}^{\lambda_{a_4}t}
\end{pmatrix}$$

and

$$\bar{J}_B=\begin{pmatrix}
\mathrm{e}^{et}\cos(ft) & \mathrm{e}^{et}\sin(ft) & 0 & 0 & 0 & 0 & 0 & 0\\
-\mathrm{e}^{et}\sin(ft) & \mathrm{e}^{et}\cos(ft) & 0 & 0 & 0 & 0 & 0 & 0\\
0 & 0 & \mathrm{e}^{\lambda_{b_1}t} & 0 & 0 & 0 & 0 & 0\\
0 & 0 & 0 & \mathrm{e}^{\lambda_{b_2}t} & 0 & 0 & 0 & 0\\
0 & 0 & 0 & 0 & \mathrm{e}^{\lambda_{b_3}t} & 0 & 0 & 0\\
0 & 0 & 0 & 0 & 0 & \mathrm{e}^{\lambda_{b_4}t} & 0 & 0\\
0 & 0 & 0 & 0 & 0 & 0 & \mathrm{e}^{\lambda_{b_5}t} & 0\\
0 & 0 & 0 & 0 & 0 & 0 & 0 & \mathrm{e}^{\lambda_{b_6}t}
\end{pmatrix}.$$

APPENDIX D: DEFINITIONS OF H_i AND G_i

$$H_1(t_1,t_2,t_3,t_4)=(I-\mathrm{e}^{At_4}\mathrm{e}^{Bt_3}\mathrm{e}^{At_2}\mathrm{e}^{Bt_1})^{-1},\qquad H_2(t_1,t_2,t_3,t_4)=(I-\mathrm{e}^{Bt_1}\mathrm{e}^{At_4}\mathrm{e}^{Bt_3}\mathrm{e}^{At_2})^{-1},$$

$$H_3(t_1,t_2,t_3,t_4)=(I-\mathrm{e}^{At_2}\mathrm{e}^{Bt_1}\mathrm{e}^{At_4}\mathrm{e}^{Bt_3})^{-1},\qquad H_4(t_1,t_2,t_3,t_4)=(I-\mathrm{e}^{Bt_3}\mathrm{e}^{At_2}\mathrm{e}^{Bt_1}\mathrm{e}^{At_4})^{-1}.$$

where I denotes the identity 8×8 matrix.

$$G_1(t_1,t_2,t_3,t_4)=\mathrm{e}^{At_4}\mathrm{e}^{Bt_3}\mathrm{e}^{At_2}\mathscr{B}(t_1)F_2+\mathrm{e}^{At_4}\mathrm{e}^{Bt_3}\mathscr{A}(t_2)F_3$$

$$+\mathrm{e}^{At_4}\mathscr{B}(t_3)F_2+\mathscr{A}(t_4)F_1,$$

$$G_2(t_1, t_2, t_3, t_4) = e^{Bt_1}e^{At_4}e^{Bt_3}\mathscr{A}(t_2)F_3 + e^{Bt_1}e^{At_4}\mathscr{B}(t_3)F_2 + e^{Bt_1}\mathscr{A}(t_4)F_1 + \mathscr{B}(t_1)F_2,$$

$$G_3(t_1, t_2, t_3, t_4) = e^{At_2}e^{Bt_1}e^{At_4}\mathscr{B}(t_3)F_2 + e^{At_2}e^{Bt_1}\mathscr{A}(t_4)F_1 + e^{At_2}\mathscr{B}(t_1)F_2 + \mathscr{A}(t_2)F_3,$$

$$G_4(t_1, t_2, t_3, t_4) = e^{Bt_3}e^{At_2}e^{Bt_1}\mathscr{A}(t_4)F_1 + e^{Bt_3}e^{At_2}\mathscr{B}(t_1)F_2 + e^{Bt_3}\mathscr{A}(t_2)F_3 + \mathscr{B}(t_3)F_2.$$

APPENDIX E: NOMENCLATURE

a_h	non-dimensional distance from airfoil mid-chord to elastic axis
b	airfoil semi-chord
c	chord
h	plunge displacement
m	airfoil mass
r_α	radius of gyration about the elastic axis
t	time
x_α	non-dimensional distance from the elastic axis to the center of mass
$C_L(\tau)$, $C_M(\tau)$	aerodynamic lift and pitching moment coefficients
$G(\xi)$, $M(\alpha)$	non-linear plunge and pitch stiffness terms
LCO	limit cycle oscillation
PSD	power spectral density
U	free stream velocity
U^*	non-dimensional velocity ($= U/b\omega_\alpha$)
U_L^*	linear flutter speed
X	system variable vector
ξ	non-dimensional plunge displacement ($= h/b$)
α	pitch angle of airfoil
$\bar{f}$	non-dimensional frequency ($= fb/U$)
ω	frequency of the motion
μ	airfoil/air mass ratio ($= m/\pi\rho b^2$)
τ	non-dimensional time ($= Ut/b$)
δ	pitch angle for the central region of the freeplay stiffness
ρ	density
ψ_1, ψ_2	constants in Wagner's function
ε_1, ε_2	constants in Wagner's function
ζ_ξ, ζ_α	viscous damping ratios in plunge and in pitch
$\bar{\omega}$	frequency ratio ($= \omega_\xi/\omega_\alpha$)
ω_ξ, ω_α	natural frequencies in plunge and in pitch
$\phi(\tau)$	Wagner's function